

# Inverse scattering series internal multiple prediction with depth dependent scalars

Andrew Iverson and Kris Innanen

## ABSTRACT

Interbed multiples continue to be detrimental to the processing and interpretation of seismic data. One prospective method to attenuate interbed multiples uses the inverse scattering series developed by Weglein et al in the 1990's. The method predicts internal multiples from the recorded data with no additional subsurface information requirements. The issue addressed in this report involves the amplitudes of the predicted internal multiples. This report displays how a depth dependent scalar can be added to the algorithm to account for errors in the prediction amplitude and improve accuracy for specific cases. The location of the scalar application in the inverse scattering series is outlined.

## INTRODUCTION

When seismic waves travel into the subsurface and cross an interface with varying mechanical properties part of the seismic energy is reflected towards the surface. If the reflection is from a single interface this is termed a primary reflection. A seismic multiple refers to an event that has reflected off multiple boundaries (Figure 1). The multiple energy is unwanted coherent noise that interferes with primary reflections and degrades the final image. For this project the type of noise targeted for removal is due to internal multiple reflections in the subsurface. It has been shown that internal multiples can negatively impact the interpretation of seismic data (Iverson, 2014).

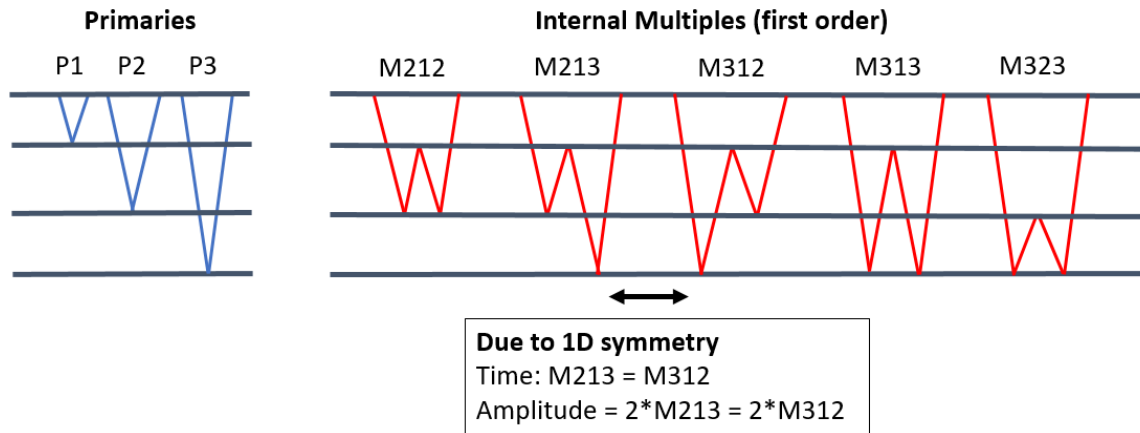


FIG. 1. (Left) Primary events for a three-layer model plus half-space (Right) First order internal multiples for the three-layer model plus half-space

Numerous methods have been utilized to attenuate multiple reflections and can be grouped into three broad categories of deconvolution, filtering and wavefield prediction (Xiao et al., 2003). Deconvolution uses the periodic nature of multiples to develop an operator to remove them, with several assumptions (Xiao et al., 2003). Filtering methods rely on the separation of primary and multiple events in various domains including f-k,

tau-p or RADON (Xiao et al., 2003). Filtering can be successful given sufficient moveout differences between primary and multiple reflections. When the moveout difference is small, multiple energy is difficult to isolate. This project implemented the Inverse Scattering Series (Weglein et al., 1997) which falls under the wavefield prediction category.

Using the Inverse Scattering Series (ISS), multiples can be predicted solely with the seismic data as input and no additional subsurface information. The method was derived using reflectivities, thus implementation on band limited data must be done cautiously. This is overcome through a parameter epsilon which accounts for the seismic bandwidth and any other lower-higher-lower criteria issues. ISS correctly predicts the time the multiples occur but the predicted amplitude will be incorrect. The amplitude errors are often rectified with the application of a shaping filter through the process of adaptive subtraction (Keating et al., 2015). What is outlined is a method to correct the amplitude issues and reduce the load on the adaptive subtraction.

## THEORY

The scattering series describes the relationship between the physical properties of an actual and reference medium and the impulse response of that reference and actual medium (Weglein et al., 1997). Where the inverse scattering series takes the resulting wavefield, the reference medium and reference wavefield to give the perturbation operator (Weglein et al., 1997). By writing the scattering equation as a series the given order of multiple is represented from the higher order terms of the series. This equation can predict higher order events from the resulting wavefield alone but at this stage it will predict events that are not interbed multiples. A subset of the series order is selected to obey a lower-higher-lower criterion (Weglein et al., 1997). This ensures that the multiples predicted are from a set of sub events that are initially deeper in the subsurface then shallower, then deeper. Giving equation (1) below to predict interbed multiples from the seismic data alone.

$$\begin{aligned}
 & b_3(k_g, k_s, \omega) \\
 &= \frac{1}{(2\pi)^2} \iint_{-\infty}^{\infty} dk_1 e^{-iq_1(\epsilon_g - \epsilon_s)} dk_2 e^{iq_2(\epsilon_g - \epsilon_s)} \int_{-\infty}^{\infty} dz_1 e^{i(q_g + q_1)z_1} b_1(k_g, -k_1, z_1) \\
 & \quad \times \int_{-\infty}^{z_1 - \epsilon} dz_2 e^{-i(q_1 + q_2)z_2} b_1(k_1, -k_2, z_2) \int_{z_2 + \epsilon}^{\infty} dz_3 e^{i(q_2 + q_s)z_3} b_1(k_2, -k_s, z_3), \quad (1)
 \end{aligned}$$

Where in equation (1)

$$q_x = \frac{\omega}{c_0} \sqrt{1 - \frac{k_x^2 c_0^2}{\omega^2}}, \quad (2)$$

$b_3$  is the interbed multiple prediction,  $b_1$  is the prepared input data,  $q_x$  is the vertical wavenumber and  $\epsilon$  is the depth below free surface of the source (s) and receiver (g),  $k$  is the Fourier conjugate variable,  $z_1, z_2$  and  $z_3$  are the depths chosen to satisfy lower-higher-lower relationship and  $\epsilon$  is the search limiting parameter (Sun and Innanen, 2014). Epsilon is used to account for the bandwidth of the data which is used in the integration limits. This sets a limit on the distance the multiple must have traveled to prevent the method from predicting multiples within the wavelength of a single wavelet.

Equation (1) predicts seismic multiples in the Fourier domain through the specific combinations of events which obey the lower-higher-lower relationship in the data. In time this is equivalent to a combination of convolutions and correlations of these specific events that satisfy the location criteria. It is shown schematically how two deeper events can be convolved relative to a shallower event, which can be correlated to mimic the equivalent multiple (Figure 2). More simply two deeper events can be added, and then the shallower event subtracted to create the multiple.

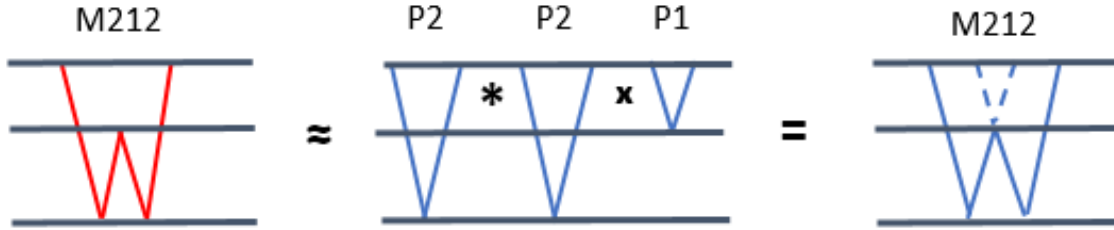


FIG. 2. Schematic displaying how a multiple can be replicated with a combination of primaries through a convolution (\*) and correlation (x)

### Reduction to 1D Pseudo-depth domain

Equation (1) can also be reduced to a 1D prediction algorithm (Eaid et al. 2016). This 1D version will be used to introduce how the method calculates multiples. The 1D version of the algorithm assumes that there is no spatial dimension.

$$k_g = k_s = 0, \quad (3)$$

Then  $q_g$  reduces to

$$q_g = 2 \frac{\omega}{c_0}, \quad (4)$$

The original 2D equation (1) then reduces to the following the 1D equation (5)

$$b_3(\omega) = \int_{-\infty}^{\infty} dz_1 e^{i2\frac{\omega}{c_0}z_1} b_1(z_1) \int_{-\infty}^{z_1-\epsilon} dz_2 e^{-i2\frac{\omega}{c_0}z_2} b_1(z_2) \int_{z_2+\epsilon}^{\infty} dz_3 e^{i2\frac{\omega}{c_0}z_3} b_1(z_3), \quad (5)$$

The data preparation for the 1D version of the algorithm is displayed (Eaid et al. 2016). First by first Fourier transforming the input data

$$d(t) \xrightarrow{F} D(\omega), \quad (6)$$

Then using the follow change of variables from frequency to wavenumber

$$k_z = \frac{2\omega}{c_0}, \quad (7)$$

Then Inverse Fourier transformed to pseudo depth

$$D(k_z) \xrightarrow{iF} b_1(z), \quad (8)$$

Where the pseudo-depth variable  $z$  is

$$z = \frac{c_0 t}{2}, \quad (9)$$

In practice when implementing the method numerically the 1D version of the algorithm can be further simplified using a Heaviside step function (Eaid et al. 2016). For 1D this gives the equation (10). This has not altered the effectiveness of the equation as no new assumptions have been made, it simply reduces the computational expense (Eaid et al. 2016).

$$b_3(\omega) = \int_{-\infty}^{\infty} dz_1 e^{-i2\frac{\omega}{c_0}z_1} b_1(z_1) \left[ \int_{z_1+\varepsilon}^{\infty} dz_2 e^{i2\frac{\omega}{c_0}z_2} b_1(z_2) \right]^2, \quad (10)$$

### 1D Analytic Multiple Prediction Example

Next a 1D analytic example will be completed to demonstrate how the method predicts multiples from an input data set. Using a geologic model that has two layers plus a half space the resulting seismic trace will contain two primary events and a multiple train with the first order multiple referred to as M212 (Figure 2). Giving the following amplitudes for the seismic trace.

$$\begin{aligned} P_1 &= R_1 \\ P_2 &= T_{01}R_2 T_{10} \\ M_{212} &= T_{01}R_2(-R_1) R_2 T_{10}, \end{aligned} \quad (11)$$

Where R is the zero-offset reflection coefficient, T is the transmission coefficient and P and M are the primary and multiple events. With corresponding traveltimes,

$$\begin{aligned} t_1 &= 2\frac{z_1}{v_1} \\ t_2 &= 2\frac{z_1}{v_1} + 2\frac{z_2-z_1}{v_2} \\ t_{212} &= 2\frac{z_1}{v_1} + 4\frac{z_2-z_1}{v_2}, \end{aligned} \quad (12)$$

Then the input data  $b_1$  will be given as follows

$$b_1(z) = P_1\delta(z - z_1) + P_2\delta(z - z_2) + M_{212}\delta(z - z_{212}) + \text{Higher Order IM} \quad (13)$$

Inserting this into the innermost integral of equation (10) where  $\hat{z}$  is used to denote the integration variable and distinguish from z for the pseudo-depths of the layers.

$$\begin{aligned} I_1(\hat{z}_1) &= \int_{\hat{z}_1+\varepsilon}^{\infty} d\hat{z}_2 e^{i2\frac{\omega}{c_0}\hat{z}_2} [P_1\delta(\hat{z}_2 - z_1) + P_2\delta(\hat{z}_2 - z_2) + M_{212}\delta(\hat{z}_2 - z_{212}) \\ &\quad + \text{Higher Order IM}], \end{aligned} \quad (14)$$

Solving the innermost integral gives the following result

$$= \begin{cases} P_1 e^{i2\frac{\omega}{c_0}z_1}, & z_1 > \hat{z}_1 + \varepsilon \\ 0, & z_1 < \hat{z}_1 + \varepsilon \end{cases} + \begin{cases} P_2 e^{i2\frac{\omega}{c_0}z_2}, & z_2 > \hat{z}_1 + \varepsilon \\ 0, & z_2 < \hat{z}_1 + \varepsilon \end{cases} + \begin{cases} M_{212} e^{i2\frac{\omega}{c_0}z_{212}}, & z_{212} > \hat{z}_1 + \varepsilon \\ 0, & z_{212} < \hat{z}_1 + \varepsilon \end{cases} + \dots \quad (15)$$

Can also be written as followed with the use of Heaviside step function

$$I_1(\hat{z}_1) = P_1 e^{i2\frac{\omega}{c_0}z_1} H[z_1 - (\hat{z}_1 + \varepsilon)] + P_2 e^{i2\frac{\omega}{c_0}z_2} H[z_2 - (\hat{z}_1 + \varepsilon)] \\ + M_{212} e^{i2\frac{\omega}{c_0}z_{212}} H[z_{212} - (\hat{z}_1 + \varepsilon)], \quad (16)$$

Squaring equation (16) will give the result to be used in the next integral from equation (10)

$$I_2(\hat{z}_1) = P_1^2 e^{i2\frac{\omega}{c_0}2z_1} H[z_1 - (\hat{z}_1 + \varepsilon)] + 2P_1P_2 e^{i2\frac{\omega}{c_0}(z_2+z_1)} H[z_1 - (\hat{z}_1 + \varepsilon)] \\ + P_2^2 e^{i2\frac{\omega}{c_0}2z_2} H[z_2 - (\hat{z}_1 + \varepsilon)] + \dots, \quad (17)$$

Inserting equation (17) into the outermost integral in equation (10) integral gives the following

$$b_3(\omega) = \int_{-\infty}^{\infty} d\hat{z}_1 e^{-i2\frac{\omega}{c_0}\hat{z}_1} [P_1\delta(\hat{z}_1 - z_1) + P_2\delta(\hat{z}_1 - z_2) + M_{212}\delta(\hat{z}_1 - z_{212}) \\ + \text{Higher Order IM}] \times [P_1^2 e^{i2\frac{\omega}{c_0}2z_1} H[z_1 - (\hat{z}_1 + \varepsilon)] \\ + 2P_1P_2 e^{i2\frac{\omega}{c_0}(z_2+z_1)} H[z_1 - (\hat{z}_1 + \varepsilon)] + P_2^2 e^{i2\frac{\omega}{c_0}2z_2} H[z_2 - (\hat{z}_1 + \varepsilon)] + \dots], \quad (18)$$

Truncating this to only include the primary events gives

$$b_3(\omega) = \int_{-\infty}^{\infty} d\hat{z}_1 e^{-i2\frac{\omega}{c_0}\hat{z}_1} [P_1\delta(\hat{z}_1 - z_1) + P_2\delta(\hat{z}_1 - z_2)] \times \left[ P_1^2 e^{i2\frac{\omega}{c_0}2z_1} H[z_1 - (\hat{z}_1 + \varepsilon)] + 2P_1P_2 e^{i2\frac{\omega}{c_0}(z_2+z_1)} H[z_1 - (\hat{z}_1 + \varepsilon)] + P_2^2 e^{i2\frac{\omega}{c_0}2z_2} H[z_2 - (\hat{z}_1 + \varepsilon)] \right], \quad (19)$$

Rearranging for both primaries

$$b_3(\omega) = \int_{-\infty}^{\infty} d\hat{z}_1 e^{-i2\frac{\omega}{c_0}\hat{z}_1} P_1\delta(\hat{z}_1 - z_1) \times \left[ P_1^2 e^{i2\frac{\omega}{c_0}2z_1} H[z_1 - (\hat{z}_1 + \varepsilon)] + 2P_1P_2 e^{i2\frac{\omega}{c_0}(z_2+z_1)} H[z_1 - (\hat{z}_1 + \varepsilon)] + P_2^2 e^{i2\frac{\omega}{c_0}2z_2} H[z_2 - (\hat{z}_1 + \varepsilon)] \right] \\ + \int_{-\infty}^{\infty} d\hat{z}_1 e^{-i2\frac{\omega}{c_0}\hat{z}_1} P_2\delta(\hat{z}_1 - z_2) \left[ P_1^2 e^{i2\frac{\omega}{c_0}2z_1} H[z_1 - (\hat{z}_1 + \varepsilon)] + 2P_1P_2 e^{i2\frac{\omega}{c_0}(z_2+z_1)} H[z_1 - (\hat{z}_1 + \varepsilon)] + P_2^2 e^{i2\frac{\omega}{c_0}2z_2} H[z_2 - (\hat{z}_1 + \varepsilon)] \right], \quad (20)$$

Then solving gives the following result

$$\begin{aligned}
b_3(\omega) = & P_1^3 e^{i2\frac{\omega}{c_0}z_1} H[z_1 - (z_1 + \varepsilon)] + 2P_1^2 P_2 e^{i2\frac{\omega}{c_0}z_2} H[z_1 - (z_1 + \varepsilon)] \\
& + P_1 P_2^2 e^{i2\frac{\omega}{c_0}(2z_2 - z_1)} H[z_2 - (z_1 + \varepsilon)] + P_1^2 P_2 e^{i2\frac{\omega}{c_0}(2z_1 - z_2)} H[z_1 - (z_2 + \varepsilon)] \\
& + 2P_1 P_2^2 e^{i2\frac{\omega}{c_0}z_1} H[z_1 - (z_2 + \varepsilon)] + P_2^3 e^{i2\frac{\omega}{c_0}z_2} H[z_2 - (z_2 + \varepsilon)], \quad (21)
\end{aligned}$$

Note that the above Heaviside step functions will give the following

$$\begin{cases} 0, H[z_1 - (z_1 + \varepsilon)] \text{ for all } \varepsilon \\ 0, H[z_1 - (z_2 + \varepsilon)] \text{ for all } \varepsilon \\ 0, H[z_2 - (z_2 + \varepsilon)] \text{ for all } \varepsilon \\ 1, H[z_2 - (z_1 + \varepsilon)] \text{ for } \varepsilon < (z_2 - z_1), \end{cases} \quad (22)$$

Resulting in the final truncated solution in the Fourier domain

$$b_3(\omega) = P_1 P_2^2 e^{i2\frac{\omega}{c_0}(2z_2 - z_1)}, \quad (23)$$

Then applying the inverse Fourier transform gives.

$$b_3(t) = R_1 T_{01} R_2 T_{10} T_{01} R_2 T_{10} \delta(t - (2t_2 - t_1)), \quad (24)$$

Comparing this back to the multiple defined in equation (11) and (12) the ISS has predicted the time of the multiple exactly. The amplitude prediction is off by the transmission coefficients from both the downgoing ( $T_{01}$ ) and upgoing ( $T_{10}$ ) component across the multiple generating horizon (interface 1). The error in the amplitude arises from the outermost integral and is a function of the “generator” depth  $\hat{z}_1$  in the analytic example, or  $z_1$  from equation (10).

## 1D INTERNAL MULTIPLE PREDICTION

The 1D version of the algorithm is implemented on a simple geologic model where the velocities and depths are displayed below (Figure 3). The modeling and subsequent prediction is completed using a constant density. Model parameters were chosen to produce multiples that have high amplitudes due to the large impedance contrasts and occur in distinct locations from the primary events. The goal is to evaluate the accuracy of the ISS prediction on a simple 1D model.

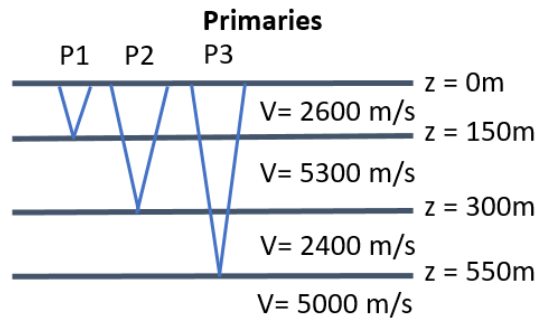


FIG. 3. Velocity and depth model used for the 1D prediction.

The primaries and first order multiples were computed using zero offset reflection and transmission coefficients to create a reflectivity series with sample rate 0.0001s, then convolved with a 40Hz Ricker wavelet and resampled to 0.002s to create the seismic trace (Figure 4).

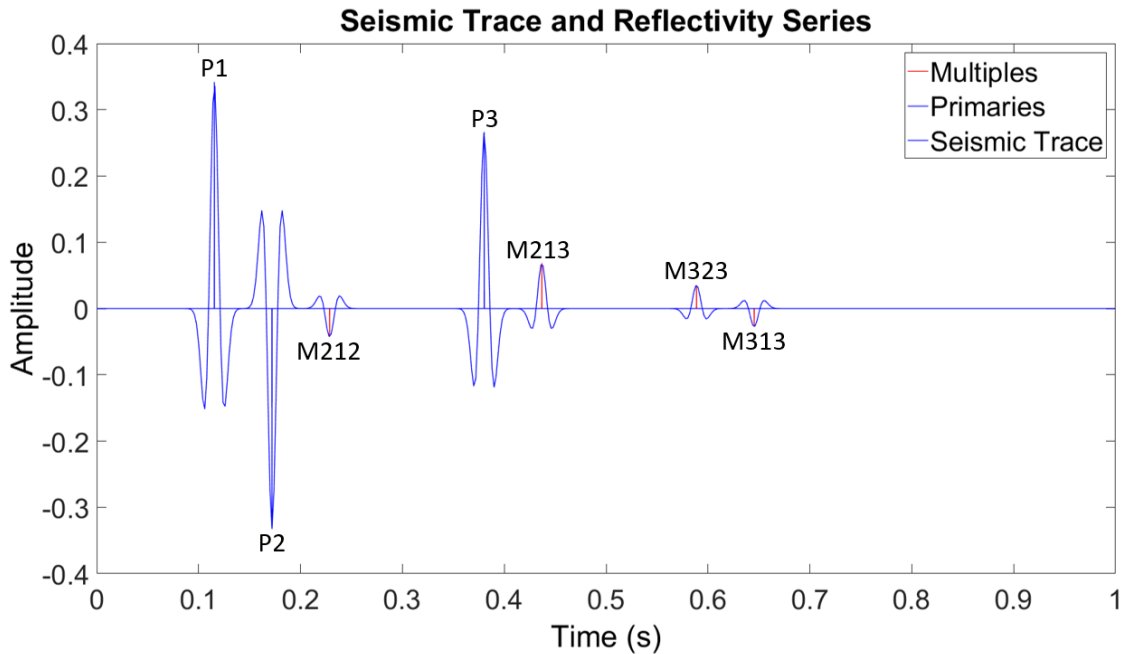


FIG. 4. Reflectivity series for primaries and first order multiples and seismic trace

The resulting prediction is displayed (Figure 5), this prediction was completed using an epsilon value of 15 due to the bandwidth of the data. The output from the prediction requires a single global scalar to place the prediction at approximately the same amplitude as the input trace. In this example, the global scalar was calculated by matching the maximum amplitude of the first multiple (M212) to the prediction. In practice the subsurface model is unknown, as are which events are primaries and multiples, but an estimate for a single scalar would still be required. The trace was also shifted by a single sample to further improve the prediction. Displayed is the input trace overlain by the result of the internal multiple prediction multiplied by negative one to examine the match to the input data (Figure 5).

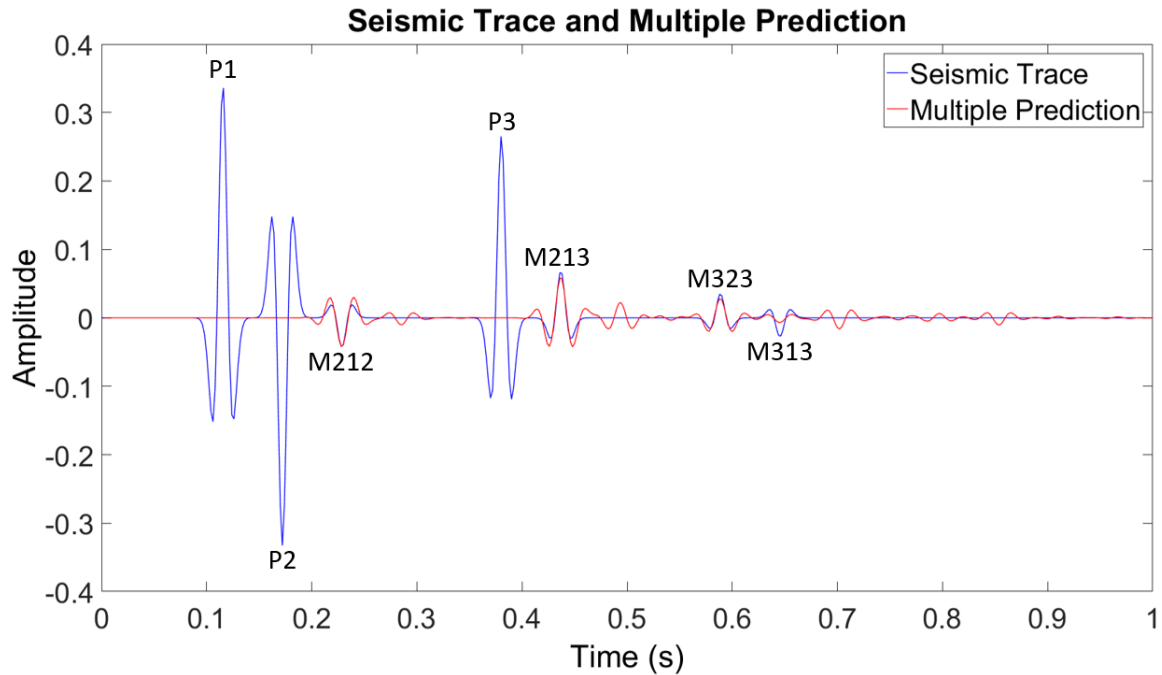


FIG. 5. Input seismic trace and 1D internal multiple prediction

All of the multiples from the input model have been predicted correctly in time and the primaries have not been predicted. There are also predictions of higher order multiples, which are the additional wavelets that do not correspond with the input trace as these were not originally modeled. The wavelets on the prediction appear to have been altered relative to the input trace and now contain additional sidelobes. This is due to the autocorrelation of the band limited data.

### Autoconvolution of a Wavelet

A 40Hz Ricker wavelet is taken and autoconvolved to display the impact of this on the prediction (Figure 6).

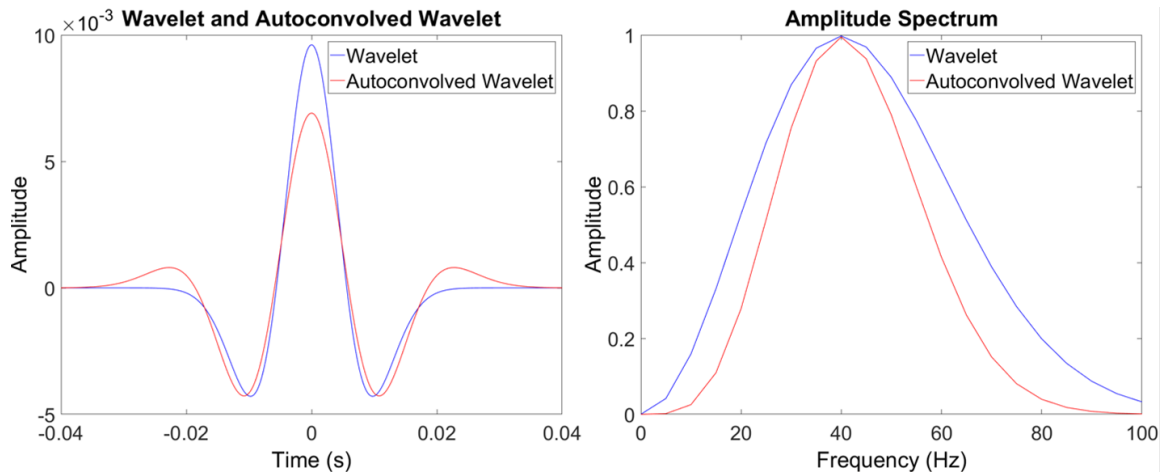


FIG. 6. (Left) 40 Hz Ricker wavelet and autoconvolution of the wavelet. (Right) amplitude spectrum of the 40 Hz Ricker wavelet and autoconvolution of the wavelet

The result in the time domain is both the slight decrease in amplitude of the wavelet and the addition of the sidelobes. In the amplitude spectrum, the dominant frequency has remained the same for the prediction but the amplitude has decreased at both the high and low end of the frequency spectrum.

### Algorithm Order of Operations

In practice this algorithm is implemented numerically by solving each frequency for all possible pseudo depth locations of multiple generators. From equation (10) the pseudo-depth location of the outermost integral varies at the location of the downward generator. The pseudo code for how this is implemented is shown (Figure 7). Equation (24) displayed that the amplitude that is predicted will be in error by the transmission across the downward generator. What is proposed is a change to the order of operations for the numerical application of the internal multiple prediction. The change proposed is to predict all frequencies for each downward generator (Figure 7). This produces a natural location to alter the equation to account for the transmission loss at the generator. This is done at the last step where the prediction at a given depth  $z$  is multiplied by the scalar  $\varphi(z)$ . Also proposed is the recording of a matrix of predictions for each pseudo-depth generator. Then to obtain the final prediction simply sum over all pseudo-depth predictions.

<pre> for ik = kz1:kzmax {     lpos = exp(i*kzPos(ik)*z)     lneg = exp(-i*kzPos(ik)*z)     intPos = b1z*lpos;     intNeg = b1z*lneg;      for iz = z1:zmax {          inner = sum(intPos(iz+ε:zmax))         pred(ik) = pred(ik) + intNeg(iz)*inner*inner     } } </pre>	<pre> for iz = z1:zmax {      for ik = kz1:kzmax {          lpos = exp(i*kzPos(ik)*z)         lneg = exp(-i*kzPos(ik)*z)         intPos = b1z*lpos;         intNeg = b1z*lneg;          inner = sum(intPos(iz+ε:zmax))         pred(iz, ik) = intNeg(iz)*inner*inner     }     pred(iz, :) = pred(iz, :)*φ(iz) } spred(ik) = sum(pred(iz, ik)) </pre>
---	---

FIG. 7. (Left) Summing over wavenumber then depth (Right) proposed order of operations alteration summing over depth then wavenumber with scalar applied to give scaled prediction

This additional scalar can be displayed in either the frequency domain as

$$sb_3(z_1, \omega) = \varphi(z_1) \times b_3(z_1, \omega), \quad (25)$$

Where  $sb_3$  is the scaled version of  $b_3$ . Or applied in the time domain after inverse Fourier transforming gives

$$sb_3(z_1, t) = \varphi(z_1) \times b_3(z_1, t), \quad (26)$$

One concern that immediately arises from applying a scalar to the prediction is that some subsurface information must be assumed. As the scalar is a precalculated depth dependent value to account for losses. One of the key benefits of the original method is that it is data driven. If some prior knowledge of the subsurface is now assumed then this may be too significant an alteration to the original equation. What was shown from the analytic example is that the difference was due to transmission losses which this can now theoretically be accounted for. This could also be applied to any other losses such as those due to geometric spreading or attenuation through a more complex scalar. The goal of this alteration is to attempt to correctly calculate the amplitudes with the utilization of additional physics to reduce the load on adaptive subtraction.

For the previous geologic model the scalar is calculated by using the velocities and depths from the model and calculating the transmission loss with depth. In practice this could be implemented with a sonic log to calculate the transmission loss. For this example, the first and last values were extrapolated to zero depth and final depth and the intermediate values were linearly interpolated. A block model was not used so that there would not be a step change at the location of the downward generator as this would significantly impact the amplitude within the width of the wavelet. The Transmission loss is displayed (Figure 8). To apply this to the prediction, take one over this to create  $\phi$  or directly divide the transmission loss.

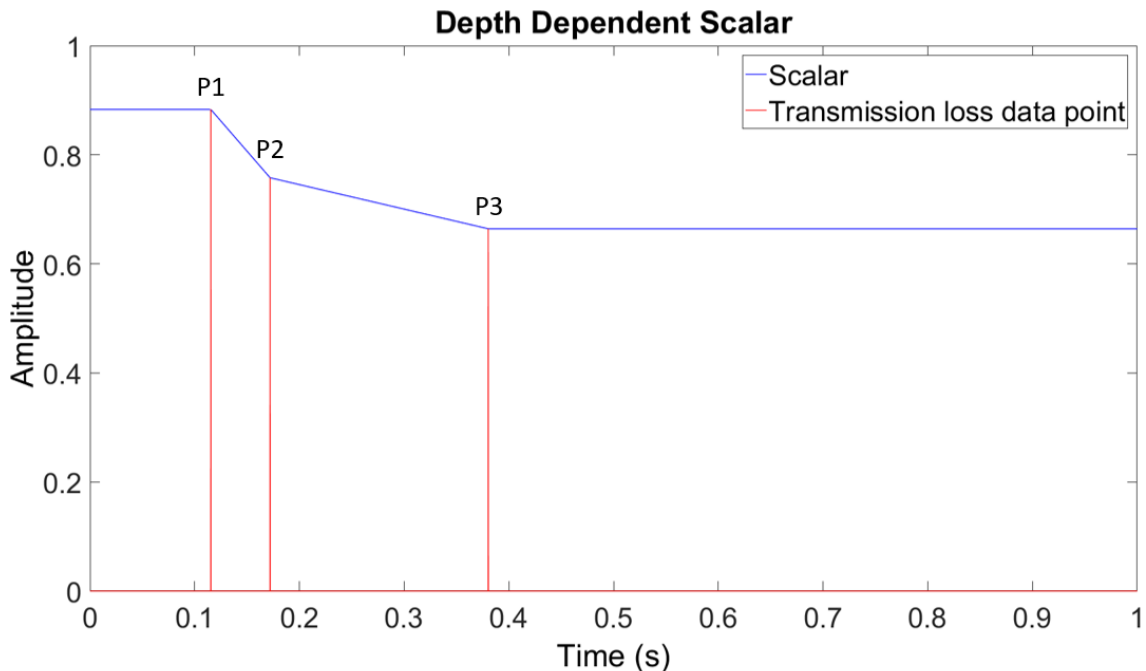


FIG. 8. Transmission loss scalar for internal multiple prediction.

The result from both the original prediction and the scalar applied prediction is displayed (Figure 9). Similarly, to the previous example both have a single global scalar applied to compare the differences. This global scalar was computed by matching the maximum amplitude of the first multiple (M212). Both versions of the method have

accurately predicted all multiples in the data. There exist small variations throughout the trace but in general both predictions are comparable. The minimal differences between the two reflect the small adjustment made to the amplitude of the prediction. The largest impact of the depth dependent scalar should be located at the internal multiple M323 (Figure 9). This internal multiple will have transmission effects due to the second interface not previously accounted for. From Figure 9 the peak amplitude of the multiple prediction for the scaled version has better accounted for extra transmission terms relative to the unscaled version. There is also an increased amplitude of the sidelobes. In Figure 9 there is a slightly lower amplitude prediction for the multiple M313. Thus this depth dependent scalar has improved the prediction for one multiple and been detrimental to another.

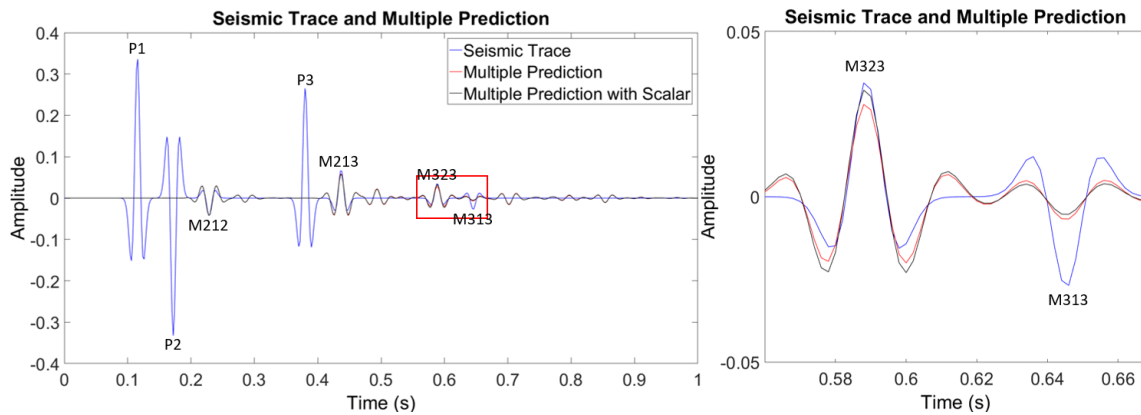


FIG. 9. (Left) Trace with both scaled and unscaled predictions (Right) Zoom in on two multiples M323 and M313

## Second Order Multiple Predictions

The theory section displayed how the algorithm predicts multiples with a combination of primaries from the input trace. It was also noted that the analytic prediction was truncated to only include the primary events. When internal multiples are present in the data these events will be used to predict the higher order multiples. These higher order multiple predictions must still obey the lower-higher-lower relationship. Displayed is a schematic of how the algorithm will produce a 2<sup>nd</sup> order internal multiple from the first order multiples and primaries in the trace (Zhang & Shaw, 2010) (Figure 10).

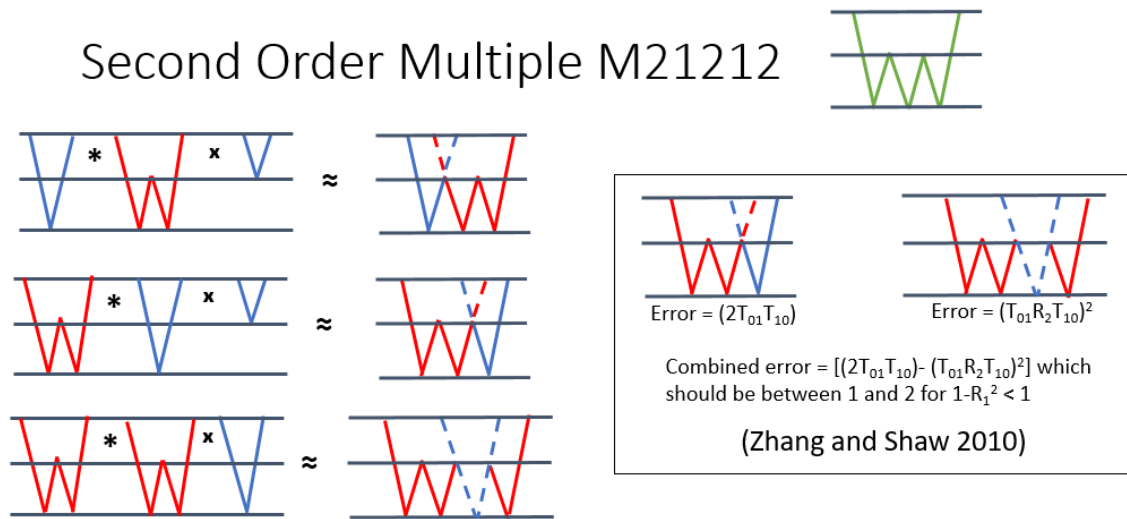


FIG. 10. Displaying the algorithm computing second order multiples with convolution (\*) and correlation (x)

Schematically displayed is how higher order multiples are predicted in an equivalent manner by combining a subset of events, however the problem that arises is that second order multiples are generally overpredicted. This further complicates the amplitude prediction issue as first order multiples are generally underpredicted and the second order multiples are over predicted (Zhang & Shaw, 2010).

Displayed in Figure 11 is the seismic trace using the previous geologic model with both first and second order multiples modeled. At the location of the underpredicted M313 multiple from Figure 9 there is a second order multiple at this location with the opposite sign relative to the first order multiple. Thus, this event may not have been as underpredicted as observed, due to a higher order multiple that was not originally modeled. In practice the amplitude correction necessary is more complicated than the multiplication of a single depth dependent scalar.

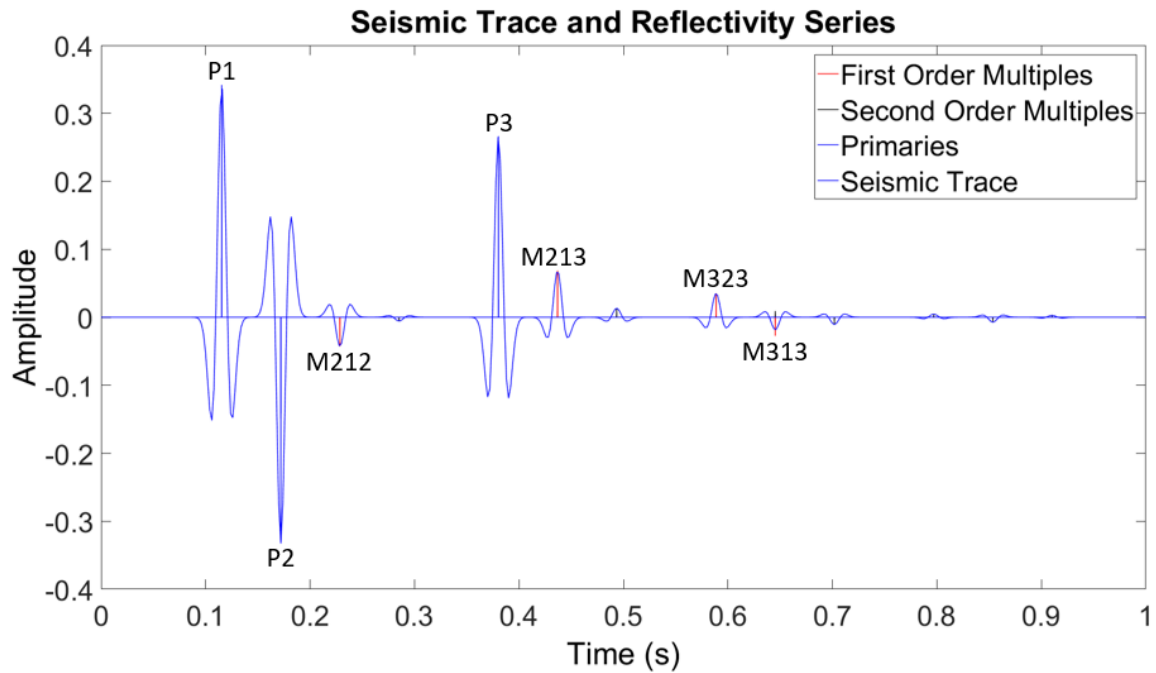


FIG. 11. Reflectivity series and trace for primaries, first and second order multiples

This seismic trace is then applied to the internal multiple prediction algorithm using both the scaled and unscaled version (Figure 12). The prediction has done an accurate job of predicting the all multiples including the second order. The scalar impacts this prediction as it is also applied to the multiples in the trace used as a subevent, though the scalar was designed from the primary transmission loss. There are still some issues with the prediction of higher order multiples and the scalar appears to have been detrimental to the prediction in some locations.

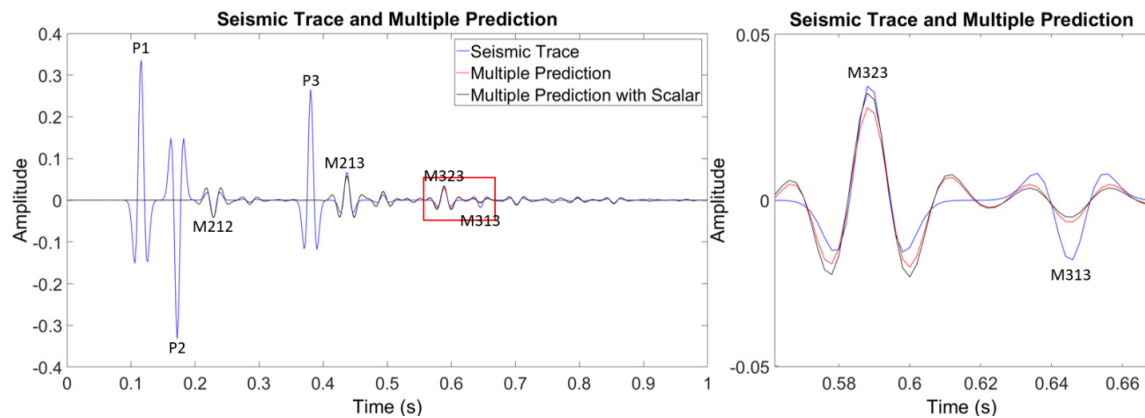


FIG. 12. (Left) Trace with both scaled and unscaled predictions with higher order multiples (Right) Zoom in on two multiples M323 and M313

Displayed is the prediction matrix in time from equation (26) (Figure 13). This two dimensional plot displays the multiple train that is the result of a layer in pseudo-depth. If we sum along all possible pseudo-depths, this creates the prediction for the entire seismic trace. This extra dimension may also allow for the calculation of a more

complete scalar to account for all amplitude issues. This also allows for a qualitative way to understand the impact of a depth dependent scalar. Combining this with the input trace, scalar and prediction gives an uncollapsed image of the multiple prediction (Figure 13). The image display how the combination of multiples of various order sum to make the final prediction.

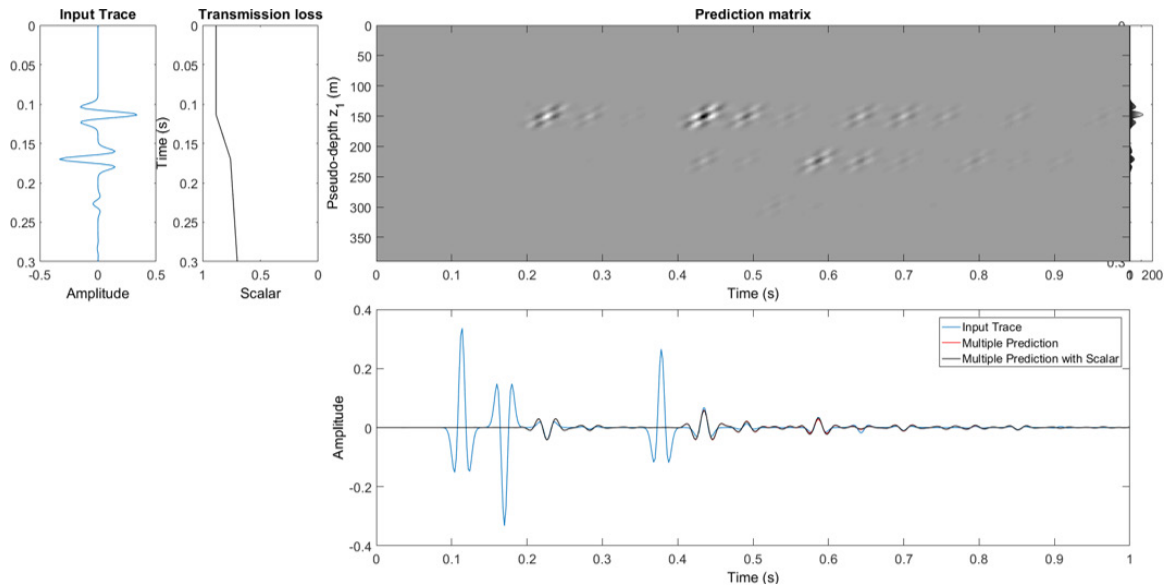


FIG. 13. (Top Left) Trace and transmission loss (Top Right) pseudo-depth and time plot with scalar applied (Bottom Right) trace and multiple prediction

## CONCLUSIONS

The objective addressed in this project was to analyze the amplitudes of the prediction to generate the cleanest possible result. A depth dependent scalar can be applied to account for losses not included in the prediction. Though it can be detrimental in the presence of significant higher order multiples. The scalar can be applied with success but it must be used cautiously and will not be beneficial to all cases. Another benefit of the change to the order of operations separate from the scalar is the ability to display the data in the pseudo-depth time plot. The pseudo-depth time plot makes it possible to visualize the multiple generators and resulting multiple train created, this also allows for the increased understanding of the final prediction which is calculated through the summation over all possible pseudo-depth generators.

## ACKNOWLEDGEMENTS

The authors would like to thank the sponsors of CREWES for the support of this work. This work was also funded NSERC through the grant CRDPJ 461179-13. Andrew Iverson would also like to thank QEII, NSERC and SEG for their support.

## REFERENCES

- Eaid, M., Sun, J., Keating, S., and Innanen, K. A., 2016, 1D and 1.5D internal multiple prediction in MatLab, CREWES Annual Report, 28.  
 Iverson, A., 2014, The impact of interbed multiples on the inversion and interpretation of prestack data, CSEG Recorder, 39(1).

- Keating, S., Sun, J., Pan, P., and Innanen, K. A., 2015, Nonstationary 11 adaptive subtraction with application to internal multiple attenuation, CREWES Annual Report, 27.
- Sun, J., and Innanen, K. A., 2016, Literature review and discussions of inverse scattering series on internal multiple prediction, CREWES Annual Report, 28.
- Weglein, A. B., Gasparotto, F. A., Carvalho, P. M., and Stolt, R. H., 1997, An inverse-scattering series method for attenuating multiples in seismic reflection data, *Geophysics*, 62(6), 1975–1989.
- Xiao, C., Bancroft, J. C., Brown, J. R., and Cao, Z., 2003, Multiple suppression: A literature review, CREWES Annual Report, 15.
- Zhang, H., and Shaw, S., 2010, 1D analytical analysis of higher order internal multiples predicted via the inverse scattering series based algorithm, SEG Technical Program Expanded Abstracts 2010, pp 3493-3498.